# Downscaling Extreme Precipitation from CMIP5 Simulations Using Historical Analogs

CHRISTOPHER M. CASTELLANO AND ARTHUR T. DEGAETANO

*Northeast Regional Climate Center, Department of Earth and Atmospheric Sciences, Cornell University, Ithaca, New York*

(Manuscript received 12 July 2016, in final form 30 June 2017)

ABSTRACT

An approach for downscaling daily precipitation extremes using historical analogs is applied to simulations from phase 5 of the Coupled Model Intercomparison Project (CMIP5). The method employs a multistep procedure in which the occurrence of extreme precipitation on a given target day is determined on the basis of the probability of extreme precipitation on that day's closest historical analogs. If extreme precipitation is expected, daily precipitation observations associated with the historical analogs are used to approximate precipitation amounts on the target day. By applying the analog method to historical simulations, the ability of the CMIP5 models to simulate synoptic weather patterns associated with extreme precipitation is assessed. Differences between downscaled and observed precipitation extremes are investigated by comparing the precipitation frequency distributions for a subset of rarely selected extreme analog days with those for all observed days with extreme precipitation. A supplemental composite analysis of the synoptic weather patterns on these rarely selected analog days is utilized to elucidate the meteorological factors that contribute to such discrepancies. Overall, the analog method as applied to CMIP5 simulations yields realistic estimates of historical precipitation extremes, with return-period precipitation biases that are comparable in magnitude to those obtained from dynamically downscaled simulations. The analysis of rarely selected analog days reveals that precipitation amounts on these days are generally larger than precipitation amounts on all days with extreme precipitation, leading to an underestimation of return-period precipitation amounts at many stations. Furthermore, the synoptic composite analysis reveals that tropical cyclones are a common feature on these rarely selected analog days.

## 1. Introduction

Extreme precipitation and flooding can have profound impacts on public infrastructure, agriculture, and human health. During the 1985–2014 period, nonstorm surge flooding was responsible for roughly $8 billion in damage (adjusted to 2014 inflation) and 80 fatalities per year in the United States. Numerous studies have documented significant increases in the frequency and magnitude of extreme precipitation in the central and eastern United States since the mid- to late-twentieth century (Kunkel et al. 1999, 2013; Kunkel 2003; DeGaetano 2009; Karl et al. 2009; Groisman et al. 2012; Heineman 2012; Villarini et al. 2013). According to the most recent assessment from the Intergovernmental Panel on Climate Change (IPCC 2014), such trends are expected to continue throughout the twenty-first century.

Although the IPCC report expresses high confidence in precipitation extremes becoming more frequent and intense in midlatitude continental regions, these predictions are based on global climate models (GCMs) that provide insufficient detail at the spatial scales relevant to hydrometeorological extremes (Christensen and Christensen 2003; Boé et al. 2006; Maraun et al. 2010). Most GCMs currently operate at spatial resolutions that are too coarse to adequately resolve certain orographic features and atmospheric processes that influence precipitation (Benestad 2010; Eden and Widmann 2014). As a result, GCMs may significantly underestimate precipitation over mountainous terrain and in areas where convective precipitation is nonnegligible. Furthermore, because simulated precipitation amounts actually represent precipitation averaged across an entire grid cell, GCMs also filter out small-scale spatial heterogeneities in precipitation. Since climate change impact assessments typically focus on point locations or finescale grids within a limited geographic domain, downscaling is required to bridge the gap between model resolution and impact area (Wilby and Wigley 1997; Murphy 1999; Wilby et al. 2004; Haylock et al.

*Corresponding author*: Christopher Castellano, cmc254@cornell.edu

DOI: 10.1175/JAMC-D-16-0250.1

2006; Benestad 2010; Maraun et al. 2010; Tryhorn and DeGaetano 2011).

Various methods for downscaling meteorological surface variables from GCMs have been explored in recent years. One such approach, originally proposed by Lorenz (1969) for operational forecasting applications, uses the concept of historical analogs. Analog methods are a subset of statistical downscaling techniques that estimate local meteorological conditions on a given target day on the basis of local observations associated with historical large-scale weather patterns that are similar to the large-scale weather pattern on the target day. In broad terms, statistical downscaling utilizes empirical relationships between large-scale atmospheric variables (predictors) and local surface variables (predictands), whereas dynamical downscaling involves running a nested high-resolution model with initial conditions and boundary values specified by an atmosphere–ocean GCM (AOGCM; Castellano and DeGaetano 2016). There is little evidence that either type yields superior results, but statistical downscaling is often preferred over dynamical downscaling because of its lower computational demands (Tryhorn and DeGaetano 2011).

Despite their simplicity, analog methods have been shown to perform as well as more sophisticated downscaling techniques and, at the very least, can provide a good benchmark for comparison (Zorita and von Storch 1999; Gutiérrez et al. 2013). Unlike statistical methods that are based on linear regression [e.g., the Statistical Downscaling Model (SDSM); Wilby et al. 2002], analog methods can easily be applied in situations in which the predictand is not normally distributed (Matulla et al. 2008). This is especially advantageous for downscaling variables such as daily precipitation. In addition, from an operational perspective, historical analogs are still used as input when forecasting extreme hydrometeorological events and assessing the potential for flooding. Nevertheless, it is worth noting that analog methods have two fundamental limitations. First, like all statistical downscaling approaches, analog methods operate under the assumption that the empirical relationships between predictors and predictands remain stable over time (Benestad 2010; Gutiérrez et al. 2013). Second, because historical observations serve as the source for the predictand estimates, analog methods cannot produce values outside the range of the existing climate record (Imbert and Benestad 2005).

Analog methods generally require three components: 1) selection of predictors, 2) a procedure for finding historical analogs on the basis of similarities in the predictor fields, and 3) a procedure for estimating predictand values. Although the selection of predictors is inherently somewhat subjective, it is important to choose variables that are physically linked to and/or are strongly correlated with the predictand, in addition to being adequately simulated by the GCMs (Wetterhall et al. 2005). For example, previous studies recommend using predictors that represent the large-scale atmospheric circulation and/or low-level moisture fields when downscaling precipitation (Matulla et al. 2008). Once the predictors have been chosen, historical analog patterns can be found via principal component analysis or direct comparison of predictor fields between target days and all possible analog days. The first approach reduces the dimensionality of atmospheric states by projecting anomalies or standardized anomalies of the predictor fields onto the leading spatial patterns of variance (e.g., Zorita and von Storch 1999; Wetterhall et al. 2005; Matulla et al. 2008). The second approach identifies suitable analogs by computing a simple dissimilarity measure (such as standardized pseudo-Euclidean distance) between predictor fields on target days and candidate analog days (e.g., Ribalaygua et al. 2013; Castellano and DeGaetano 2016). Since no single historical weather pattern is ever likely to be identical to a given target weather pattern (van den Dool 1994), the predictand value at a specific location or grid cell is often estimated as a linear combination of the observed values associated with the most similar analog patterns (e.g., van den Dool et al. 2003; Hidalgo et al. 2008; Brekke et al. 2013).

Most analog approaches that previously have been used to downscale daily precipitation, such as the bias-corrected constructed analog method (Hidalgo et al. 2008; Brekke et al. 2013), unfortunately significantly underestimate the magnitude of extreme precipitation in the central and eastern United States (Gutmann et al. 2014). Using an analog search algorithm that is similar to the one employed by Ribalaygua et al. (2013), Castellano and DeGaetano (2016) proposed a multistep procedure for downscaling daily precipitation extremes from historical analogs. First, the occurrence of extreme precipitation on a given target day was determined on the basis of the observed probability of extreme precipitation on that day's closest historical analog days. If extreme precipitation occurred on the selected analog day(s), the historical precipitation observations associated with the analog day(s) were then used to ascribe precipitation amounts on the corresponding target day. The performance of this analog method was tested using National Centers for Environmental Prediction–National Center for Atmospheric Research (NCEP–NCAR) reanalysis data (Kalnay et al. 1996) for a 50-yr trial period (1961–2010). Overall, the approach yielded encouraging results, with return-period precipitation biases that compared favorably to those produced by

dynamically downscaled historical simulations from the North American Regional Climate Change Assessment Program (NARCCAP; Mearns et al. 2009). In terms of predicting the occurrence of extreme precipitation, the analog method presented a notable improvement over using climatological probabilities and performed similar to an analog approach developed by Gao et al. (2014) that considered widespread heavy-precipitation events only.

This study applies the analog method developed by Castellano and DeGaetano (2016) to historical simulations from phase 5 of the Coupled Model Intercomparison Project (CMIP5; Taylor et al. 2012) as opposed to reanalysis data. Such an analysis is necessary to ascertain the ability of the CMIP5 GCMs to simulate the types and frequency of synoptic weather patterns that are associated with extreme precipitation and therefore to determine whether the analog method can ultimately be used to downscale future precipitation extremes. Section 2 will provide an overview of the data and method used to downscale extreme precipitation from the CMIP5 simulations. Section 3 will compare downscaled precipitation extremes estimated from the historical CMIP5 simulations with those computed from historical observations. A subsequent analysis of rarely selected analog days will be presented to explain discrepancies between downscaled and observed precipitation extremes. Last, section 4 will conclude with a brief summary of significant findings and a discussion of the potential advantages and drawbacks of this downscaling approach.

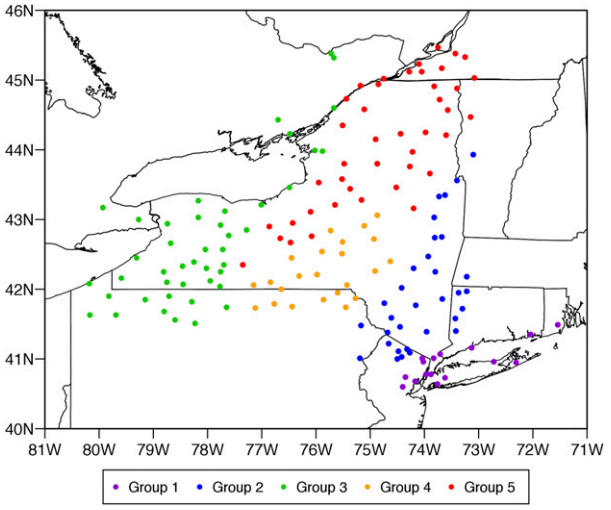


FIG. 1. Map showing the locations of the 157 GHCN stations used in this study. The different colors designate the five station groups used to assign analog precipitation amounts.

## 2. Method

### a. Observed precipitation extremes

The geographical domain for this study consists of the 157 Global Historical Climatology Network (GHCN) stations selected by Castellano and DeGaetano (2016) in their verification paper (Fig. 1). Following the methods of Wilks and Cember (1993) and Castellano and DeGaetano (2016), partial duration series (PDS) of the largest independent daily precipitation events at each station were constructed for the 1961–2010 period (the pool of candidate historical analog days) and the 1970–99 period. Next, precipitation amounts corresponding to 2-, 5-, 10-, 25-, 50-, and 100-yr return periods were computed for the 1970–99 period using the regionalized L-moments approach outlined in Castellano and DeGaetano (2016). Homogeneous regions were determined by applying a Kolmogorov–Smirnov test (DeGaetano 1998) to evaluate the likeness of the PDS distributions at different pairs of stations. A generalized extreme-value distribution was subsequently fit to each station's PDS, with regionally averaged shape and scale parameters specified for all stations in the same region. The National Weather Service is currently using L-moments regional frequency analysis (Hosking and Wallis 1997) to create a revised precipitation frequency atlas for the United States (Perica et al. 2013). Although Wilks (1993) found that a station-based beta-*P* method best captured the extreme right tail of precipitation events in the northeastern United States, the parameters of the beta-*P* distribution are very sensitive to outlier values in the PDS sample. This sensitivity leads to large spatial disparities in precipitation estimates for return periods that exceed the length of the data record. Furthermore, as Fig. 2 illustrates, this sensitivity introduces a high degree of uncertainty in the return-period estimates at certain stations.

The analysis was restricted to the 1970–99 period to allow for direct comparison with the dynamically downscaled NARCCAP simulations. Although the NARCCAP simulations were run using AOGCMs from the previous generation of IPCC models (CMIP3; Meehl et al. 2007), dynamically downscaled simulations from the Coordinated Regional Downscaling Experiment (CORDEX; Jones et al. 2011), which uses CMIP5 models as the driving AOGCMs, were not initially available. Because computing 100-yr return-period precipitation amounts on the basis of a 30-yr period involves extrapolation well beyond the length of the data record, the authors examined the reliability of these return-period estimates by comparing them with return-period values computed from the longer 1950–2005 period. Differences between the 1970–99 and 1950–2005 return-period estimates were found to be

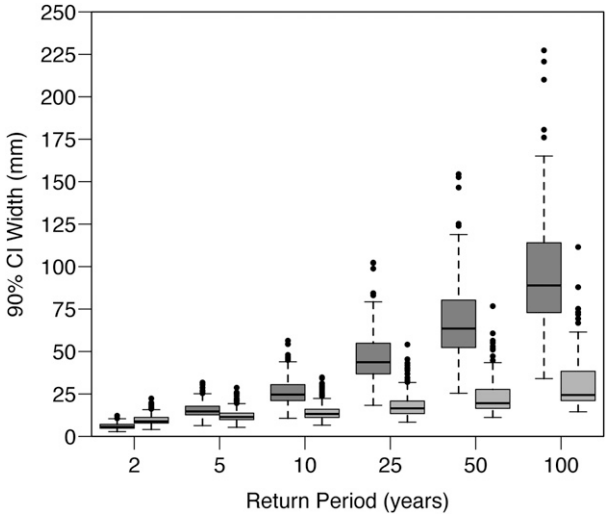


FIG. 2. Box plots showing the widths of the 90% confidence intervals for all 157 stations at different return periods. The dark-gray box plots represent the confidence intervals computed from a station-based beta-P approach, whereas the light-gray box plots represent the confidence intervals computed from the regionalized L-moments approach. Filled black circles outside the whiskers denote outliers.

negligible at most stations. Last, 90% confidence intervals for each return period were estimated using the PDS resampling procedure that was employed by Castellano and DeGaetano (2016).

### b. *Finding historical analogs*

As in Castellano and DeGaetano (2016), target days (i.e., model days) and candidate analog days (i.e., reanalysis days) were compared with one another by calculating a standardized root-mean-square error (RMSE) for the following predictor variables over the 20°N, 105°W–55°N, 50°W bounding box: 1) total precipitable water (TPW), 2) vertically integrated water vapor transport (IVT), and 3) 850-hPa relative vorticity $\zeta_{850}$. These variables were chosen after reviewing existing literature on the synoptic–dynamic processes and thermodynamic environments that are associated with extreme precipitation. Cool-season extreme-precipitation events in midlatitude regions have been linked to synoptic-scale features such as midtropospheric troughs, extratropical cyclones, and low-level poleward moisture transport (Archambault et al. 2008; Junker et al. 2008; Gao et al. 2014; Dayan et al. 2015). Studies by Maddox et al. (1979), Winkler (1988), and Konrad (1997) found that warm-season heavy-precipitation events in the central and eastern United States often occur in regions that are characterized by warm and moist air near the surface, high precipitable water, low-level moisture convergence and warm advection, and an upstream midtropospheric short-wave trough. Warm-season events with the strongest synoptic forcing are associated with extratropical cyclones and frontal boundaries. In the absence of synoptic forcing, heavy convective precipitation in a conditionally unstable air mass may occur near a midtropospheric ridge or a weak short wave aloft (Maddox et al. 1979; Heideman and Fritsch 1988; Winkler 1988). Landfalling tropical cyclones also play an important role in extreme-precipitation events in the eastern United States during late summer and early autumn (LaPenta et al. 1995; Smith et al. 2011; Kunkel et al. 2012).

On the basis of the findings from these studies, the authors examined several candidate predictor variables, including mean sea level pressure; geopotential height and relative vorticity at 850, 700, and 500hPa; 850-hPa equivalent potential temperature; TPW; and IVT. Temperature advection and moisture convergence were not included because of the poor representation of these processes by coarse-scale reanalysis data. Other variables that may be important for localized convection in situations that are characterized by conditional instability and weak synoptic forcing (e.g., convective available potential energy) were also excluded because the relevant processes cannot be adequately resolved by present-day GCMs. The combination of $\zeta_{850}$ (which may be used to identify cyclones, frontal boundaries, and short waves aloft), TPW (which may be used to represent thermodynamic environments that are favorable for heavy precipitation), and IVT (which may be used to denote regions of strong moisture transport) was ultimately found to yield the best results in the verification study conducted by Castellano and DeGaetano (2016).

Predictor fields on the candidate analog days were derived from the NCEP–NCAR reanalysis, which provides 6-hourly gridded atmospheric data at 2.5° × 2.5° horizontal resolution and 17 vertical pressure levels. Values of TPW, IVT, and $\zeta_{850}$ were computed from zonal wind, meridional wind, and specific humidity fields by using Eqs. (1)–(3):

$$\zeta_{850} = \frac{\partial v_{850}}{\partial x} - \frac{\partial u_{850}}{\partial y}, \tag{1}$$

$$\mathrm{TPW} = \frac{1}{g}\int_{1000\_\mathrm{hPa}}^{300\_\mathrm{hPa}} w\, dP, \quad \text{and} \tag{2}$$

$$\mathrm{IVT} = \frac{1}{g}\left|\int_{1000\_\mathrm{hPa}}^{300\_\mathrm{hPa}} \mathbf{v}q\, dP\right| = \left[\left(\frac{1}{g}\int_{1000\_\mathrm{hPa}}^{300\_\mathrm{hPa}} uq\, dP\right)^2 + \left(\frac{1}{g}\int_{1000\_\mathrm{hPa}}^{300\_\mathrm{hPa}} vq\, dP\right)^2\right]^{1/2}. \tag{3}$$

Here, $u$ and $v$ are the horizontal and meridional components of the total wind $\mathbf{v}$, $g$ is the gravitational

TABLE 1. Table showing the 20 CMIP5 AOGCMs, the institutions at which they were developed, and their atmospheric horizontal resolutions (degrees latitude by degrees longitude). The expansions of the model identifiers can be found online (http://www.ametsoc.org/Pubsacronymlist).

| Model identifier | Modeling center/group | Resolution |
|---|---|---|
| BCC_CSM1.1 | Beijing Climate Center, China | 2.8 × 2.8 |
| BCC_CSM1.1(m) | Beijing Climate Center, China | 1.125 × 1.125 |
| BNU-ESM | Beijing Normal University, China | 2.8 × 2.8 |
| CanESM2 | Canadian Centre for Climate Modelling and Analysis, Canada | 2.8 × 2.8 |
| CCSM4 | National Center for Atmospheric Research, United States | 0.9 × 1.25 |
| CNRM-CM5 | National Centre for Meteorological Research, France | 1.4 × 1.4 |
| CSIRO Mk3.6.0 | CSIRO, Australia | 1.875 × 1.875 |
| GFDL CM3 | Geophysical Fluid Dynamics Laboratory, United States | 2.0 × 2.5 |
| GFDL-ESM2G | Geophysical Fluid Dynamics Laboratory, United States | 2.0 × 2.5 |
| GFDL-ESM2M | Geophysical Fluid Dynamics Laboratory, United States | 2.0 × 2.5 |
| GISS-E2-H | NASA Goddard Institute for Space Studies, United States | 2.0 × 2.5 |
| GISS-E2-R | NASA Goddard Institute for Space Studies, United States | 2.0 × 2.5 |
| IPSL-CM5A-LR | L'Institut Pierre-Simon Laplace, France | 1.9 × 3.75 |
| IPSL-CM5A-MR | L'Institut Pierre-Simon Laplace, France | 1.25 × 2.5 |
| IPSL-CM5B-LR | L'Institut Pierre-Simon Laplace, France | 1.9 × 3.75 |
| MIROC-ESM | JAMSTEC/AORI/ National Institute for Environmental Studies, Japan | 2.8 × 2.8 |
| MIROC-ESM-CHEM | JAMSTEC/AORI/ National Institute for Environmental Studies, Japan | 2.8 × 2.8 |
| MIROC5 | JAMSTEC/AORI/ National Institute for Environmental Studies, Japan | 1.4 × 1.4 |
| MRI-CGCM3 | Meteorological Research Institute, Japan | 1.125 × 1.125 |
| NorESM1-M | Norwegian Climate Centre, Norway | 1.9 × 2.5 |

acceleration ($9.81\,\mathrm{m\,s^{-1}}$), $w$ is the mixing ratio, $q$ is the specific humidity, and $dP$ signifies integration with respect to pressure. Predictor fields on the target days were derived from 6-hourly CMIP5 model output for the historical climate scenario (1970–99 period only). The 20 CMIP5 AOGCMs used in this study are listed in Table 1. Before the predictor variables were computed, the raw CMIP5 data were horizontally regridded and vertically interpolated to match the horizontal and vertical resolution of the NCEP–NCAR reanalysis data. Because the GHCN stations typically report daily precipitation as the 24-h precipitation total ending at 0700 or 0800 local standard time (LST) on a given day, the predictor fields were only computed at 0000 UTC on each day.

RMSE values for a given candidate analog day–target day pair were calculated by taking the square root of the weighted mean square error across all grid points. Squared-error values at each grid point were adjusted by a weighting factor that depends on the proximity of the grid point to the study domain. As Fig. 3 illustrates, grid points nearest the study domain received the largest weighting, whereas grid points farthest from the study domain received the smallest weighting. Although the gridpoint-weighting scheme is somewhat arbitrary, this approach strikes a balance between incorporating a larger geographical area (necessary for a synoptic-scale comparison of the predictor variables) and placing an emphasis on the predictor variables over the study domain (Ribalaygua et al. 2013). The RMSE calculation is given by

$$\mathrm{RMSE}_P(x_i, a_j) = \left[ \frac{\sum_{k=1}^{N} (P_{ik} - P_{jk})^2 W_k}{\sum_{k=1}^{N} W_k} \right]^{1/2}, \qquad (4)$$

where $P_{ik}$ and $P_{jk}$ represent the value of predictor $P$ on target day $x_i$ and analog day $a_j$, respectively, at grid point $k$, $W_k$ is the weighting factor of grid point $k$, and $N$ is the total number of grid points. Standardized RMSE values were estimated by comparing the actual RMSE values with reference populations of RMSE computed from 1 000 000 randomly sampled pairs of reanalysis days. The centile values of the reference populations nearest the actual RMSE values were located, and the corresponding centiles (from 0.01 to 0.99) were taken as the standardized error values for the three predictors. Next, a dissimilarity index was obtained by calculating the mean of the three standardized error values from each predictor variable:

$$d(x_i, a_j) = \frac{1}{3} \sum_{P=1}^{3} Z_P(x_i, a_j). \qquad (5)$$

Once dissimilarity indices were found for all candidate analog days, the candidate analog days with the 30 smallest dissimilarity indices were retained.

### c. *Estimating precipitation extremes from analogs*

After finding the 30 closest historical analogs for a given target day, one of these analog days was randomly

selected, and the precipitation observations that are associated with the selected analog day were used to guide precipitation estimates on the target day. The probability of selecting a particular analog day was quantified as the ratio between the inverse of the dissimilarity index of the analog day and the inverse sum of the dissimilarity indices of all 30 of the closest analog days:

$$\pi(x_i, a_j) = \frac{[d(x_i, a_j)]^{-1}}{\sum_{k=1}^{30} [d(x_i, a_k)]^{-1}}. \quad (6)$$

To translate the analog pattern to station-based precipitation, the 157 stations were first partitioned into groups on the basis of how regularly different pairs of stations received extreme precipitation from the same meteorological event. For each unique pair of stations, the fraction of nonconcurrent PDS events [i.e., the fraction of PDS events at station A that did not occur on the same day, the previous day, or the next day at station B (and vice versa)] during the 1961–2010 period was obtained as a measure of dissimilarity between the two stations. These dissimilarity measures were used to construct a 157 × 157 distance matrix, and Ward's method of hierarchical clustering (Ward 1963) was applied to this distance matrix to identify distinct station groups. Figure 1 shows the five station groups identified by the clustering algorithm. The robustness of the station groups was validated by calculating the within-cluster dissimilarity (i.e., the mean dissimilarity measure across all unique station pairs in a given station group) and the between-cluster dissimilarity for each unique pair of station groups (i.e., the mean dissimilarity measure between all stations in one group and all stations in the second group). As expected, the within-cluster dissimilarity measures were smaller than the between-cluster dissimilarity measures.

Next, if extreme precipitation (i.e., a PDS event) occurred on the selected analog day at one or more stations in a given group, precipitation amounts were assigned to stations in the group by following the procedure outlined in Castellano and DeGaetano (2016). If only one station experienced a PDS event, the corresponding precipitation amount was randomly assigned on the basis of the percentage of group-specific single-station PDS events that occurred at each station during the 1961–2010 period. If more than one station experienced a PDS event, daily precipitation amounts were estimated at all stations using the maximum daily precipitation observation at each station during a 3-day period centered on the analog day. The largest station-specific maximum daily precipitation observation was randomly assigned to one station on the basis of the percentage of group-specific multistation PDS events during the 1961–2010 period for which each station reported the largest daily precipitation amount. All remaining maximum daily precipitation amounts were randomly assigned (assuming equal probability) to the remaining stations. Note that the largest maximum daily precipitation amount was assigned separately because the probability of receiving the largest maximum daily precipitation amount during a group-specific multistation PDS event was statistically significant at certain stations. If extreme precipitation did not occur on the selected analog day, no precipitation amounts were assigned to any stations in the group.

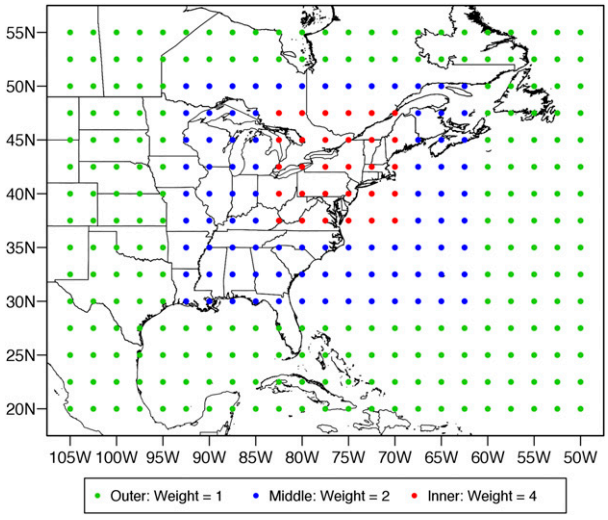


FIG. 3. Map illustrating the weighting factors assigned to the NCEP–NCAR reanalysis grid points.

After running through all target days, a new PDS (hereinafter referred to as the analog PDS) was constructed for each station by following the method employed in section 2a. First, the largest analog precipitation amounts assigned to a given station were extracted. If any two of the largest analog precipitation amounts at a given station were assigned on target days that are separated by less than seven model days, the smaller precipitation amount was replaced with the next largest unused analog precipitation amount assigned on a target day separated by at least seven days from any target day already belonging to the station's analog PDS. Last, the regionalized L-moments approach was used to calculate 2-, 5-, 10-, 25-, 50-, and 100-yr return-period precipitation amounts on the basis of the analog PDS distributions. The process of randomly selecting analog days, assigning daily precipitation amounts on model days, and estimating return-period precipitation

values was repeated 1000 times to minimize the effect of selecting only one historical analog for each target day. Medians of the 1000 simulated values were chosen to represent the final downscaled return-period precipitation estimates at each station. An overview of the primary steps in the analog downscaling procedure is illustrated by Fig. 3 in Castellano and DeGaetano (2016).

## 3. Results

### *a. Historical-period bias*

To determine whether the analog method could produce realistic estimates of historical precipitation extremes, return-period precipitation amounts obtained from the analog method were compared with return-period precipitation amounts computed from daily precipitation observations during the 1970–99 period. Figure 4 shows box plots of ensemble-mean bias in 2-, 5-, 10-, 25-, 50-, and 100-yr precipitation amounts across all 157 stations. Biases of greater or less than 1 indicate that the mean downscaled value is respectively larger or smaller than the observed value. Overall, the analog method yields realistic precipitation estimates at each return period, with median bias across all stations ranging from 0.88 to 0.97. Moreover, the percent difference between downscaled and observed 5-yr (100 yr) precipitation amounts is less than 20% for 148 (133) of the 157 stations. Approximately 52% (59%) of the 157 downscaled station values fall within the 90% confidence intervals of the observed 5-yr (100 yr) precipitation amounts (Table 2). Note that the somewhat low percentage of downscaled values that fall within the observed confidence intervals is likely an artifact of the regionalization procedure. Since the L-moments method used in this study specifies regionally averaged (as opposed to single station) shape and scale parameters for all stations in the same region, it generally produces narrow confidence intervals. To quantify the uncertainty due to the random selection of analog days, 90% confidence intervals were estimated for each CMIP5 model by computing the difference between the 5th and 95th percentiles of the 1000 simulated return-period values. This uncertainty was similar in magnitude to the intermodel variability in final downscaled return-period estimates (not shown).

As a basis for comparison, extreme-precipitation biases were also evaluated for the dynamically downscaled CORDEX and NARCCAP simulations. These simulations consist of regional climate models run at 50-km horizontal resolution and driven by CMIP5 (CORDEX) and CMIP3 (NARCCAP) AOGCMs. First, daily precipitation amounts were interpolated at each station by taking a weighted mean of the daily precipitation output over the four nearest grid cells. Gridcell weights were determined on the basis of an inverse-distance-squared relationship. Next, these interpolated daily precipitation estimates were used to construct a PDS at each station, and the corresponding return-period values were computed using the regionalized L-moments approach. Last, the simulated return-period values were adjusted by empirical areal reduction factors (ARFs; Allen and DeGaetano 2005) to convert precipitation averaged over a grid cell to point values of precipitation. Figure 5 shows box plots of ensemble-mean bias in ARF-adjusted return-period precipitation amounts for both sets of dynamically downscaled simulations.

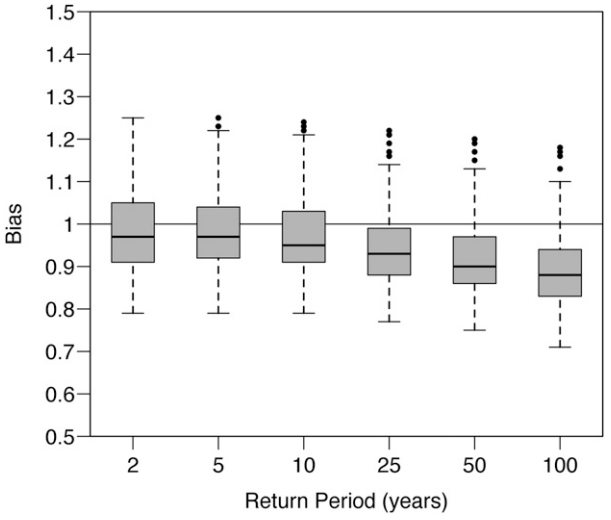


FIG. 4. Box plots illustrating the bias in ensemble-mean extreme-precipitation amounts as estimated from the analog method for the 1970–99 period at all 157 stations. Filled black circles outside the whiskers denote outliers.

In general, the analog method (Fig. 4) and the CORDEX simulations (Fig. 5a) yield extreme-precipitation biases that are similar in magnitude. Whereas the analog method tends to underestimate observed precipitation extremes by ~5%–10%, the CORDEX simulations tend to overestimate observed precipitation extremes by ~5%. The NARCCAP simulations yield the lowest return-period precipitation estimates, with median biases ranging from 0.84 to 0.93 (Fig. 5b). Moreover, the NARCCAP simulations consistently underestimate observed precipitation extremes for at least 75% of the 157 stations. The biases calculated from the CORDEX simulations exhibit larger station-to-station variability than those computed from the analog method and the NARCCAP simulations, but this result is likely due to the limited number of CORDEX

TABLE 2. Table showing the percentage of stations for which each downscaling method yielded 5- and 100-yr precipitation amounts within the 90% confidence interval bounds of the observed precipitation extremes.

| Return period | Analog method | CORDEX | NARCCAP |
|---|---|---|---|
| 5 yr | 52% | 43% | 37% |
| 100 yr | 59% | 41% | 40% |

simulations. When the downscaled precipitation extremes are compared with the 90% confidence intervals of observed precipitation extremes, it becomes clear that the analog method produces the most realistic estimates (Table 2).

In addition to examining the bias in return-period precipitation amounts, it was important to compare the downscaled and observed frequency distributions of PDS precipitation amounts in each station group. This procedure was carried out for each model by amassing all PDS precipitation amounts generated by the 1000 analog simulations at all stations in a given group. Thus, the corresponding sample size of analog PDS amounts for a given model and group is $1000 \times n \times j$, where $n$ is the length of the PDS at each station and $j$ is the number of stations in that group. The observed PDS sample for each group simply consists of the observed PDS amounts at all stations in the group during the 1970–99 period. After the analog and observed PDS distributions were constructed, exceedance probabilities were computed for various daily precipitation amounts. In this context, exceedance probability refers to the percentage of PDS values that exceed a given threshold. These exceedance probabilities are graphically illustrated in Fig. 6.

In general, the analog method yields extreme-precipitation distributions that are similar to the observed extreme-precipitation distributions. Large differences exist among the individual models, however, and the performance of the analog method varies by station group. For instance, whereas the analog PDS distributions closely mirror the observed PDS distributions in groups 3 and 5 (stations located in the western and northern sections of the study domain), the analog method tends to underestimate observed precipitation extremes in groups 1, 2, and 4 (stations located farther south and east). Among the group-1 and group-2 stations, which are primarily located in the Hudson Valley and New York City metropolitan area, at least 75% of models yield lower-than-observed exceedance probabilities for daily precipitation of more than 75 mm. Among the group-4 stations, which are located within the eastern terminus of the

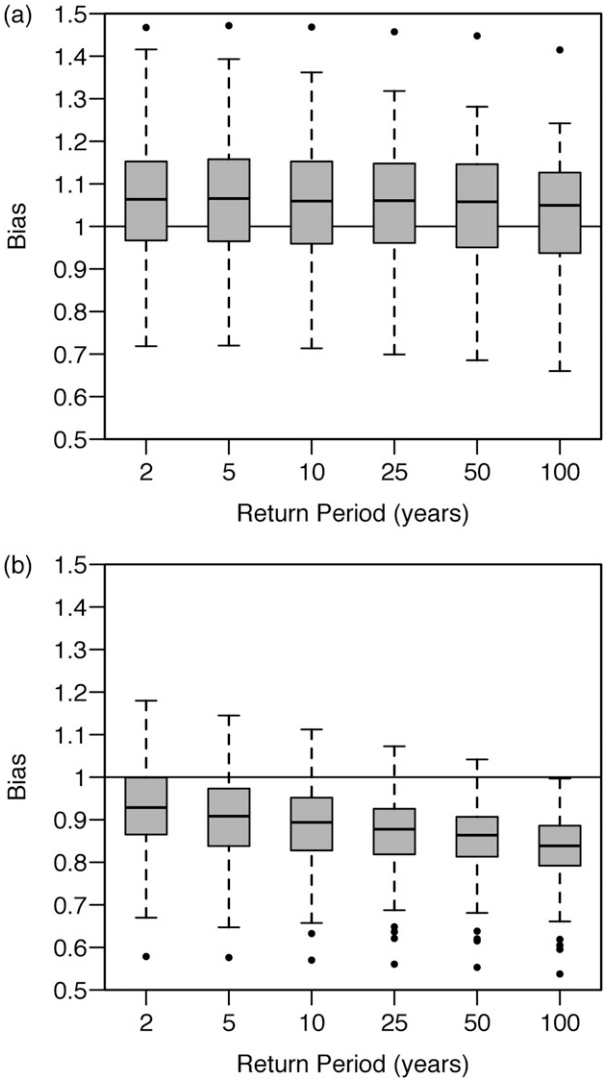


FIG. 5. As in Fig. 4, but as estimated from (a) the historical CORDEX simulations and (b) the historical NARCCAP simulations.

Allegheny Plateau, at least 75% of models yield lower-than-observed exceedance probabilities for daily precipitation of more than 50 mm. Possible explanations for these biases will be explored in greater detail in section 3b.

The monthly distributions of extreme-precipitation days predicted from the individual model simulations were compared with the monthly distribution of observed extreme-precipitation days during the 1970–99 period. From the 1000 simulations, it was first determined how often extreme precipitation was predicted on a particular model day. Next, the probability of extreme precipitation on that model day was estimated as the fraction of the 1000

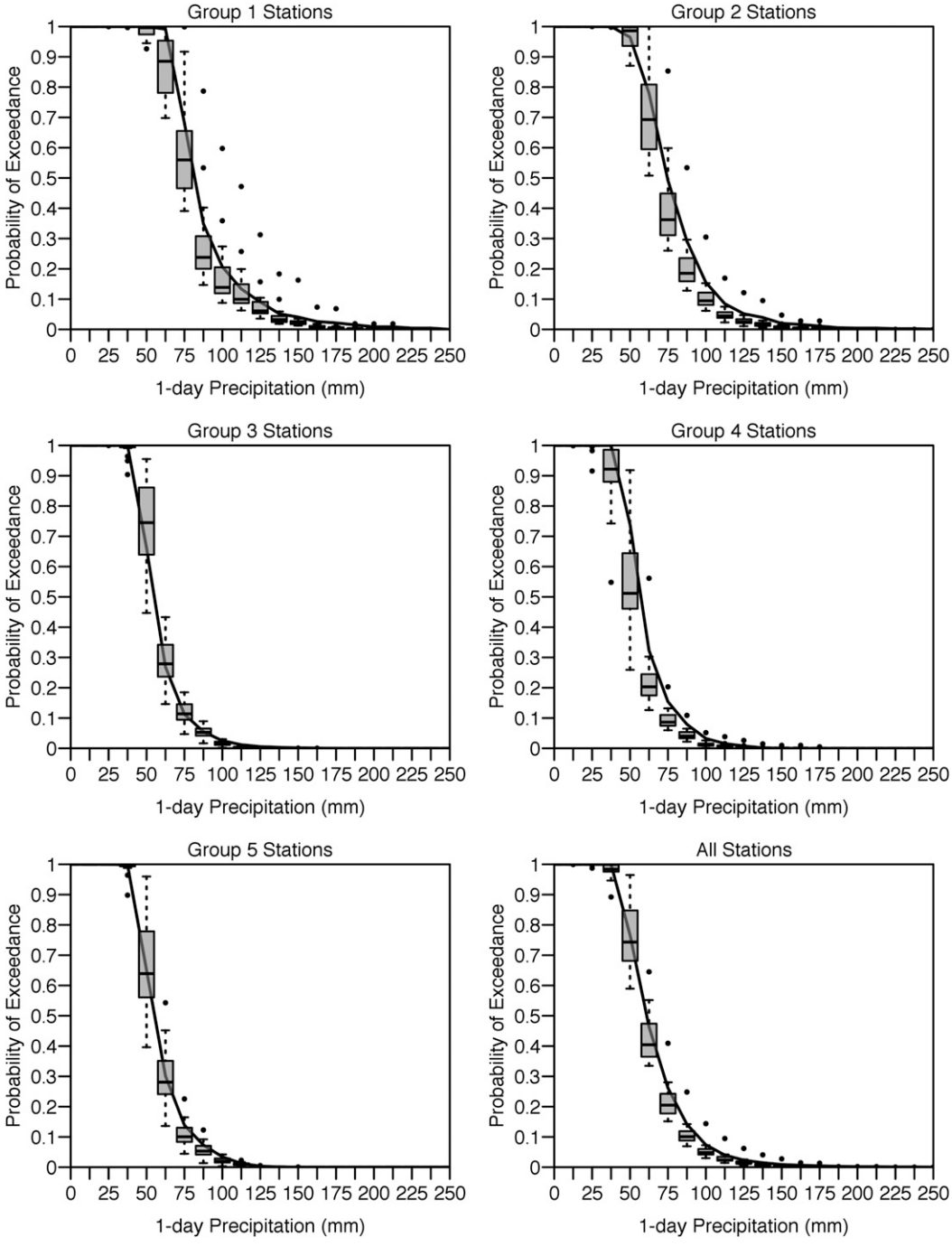


FIG. 6. Exceedance probabilities corresponding to observed (black lines) and downscaled (gray box plots) PDS precipitation amounts during the 1970–99 period. Filled black circles outside the whiskers denote outliers.

simulations for which extreme precipitation was predicted. Third, the 30-yr monthly frequencies of extreme-precipitation days were computed by taking the sum of the extreme-precipitation probabilities for all dates in each month. Side-by-side comparisons of the observed and predicted 30-yr monthly frequencies of extreme-precipitation days during the 1970–99 period for each CMIP5 model are illustrated in Fig. 7.

The analog method as applied to various CMIP5 models successfully reproduces the observed seasonal variability in extreme-precipitation days. Each model

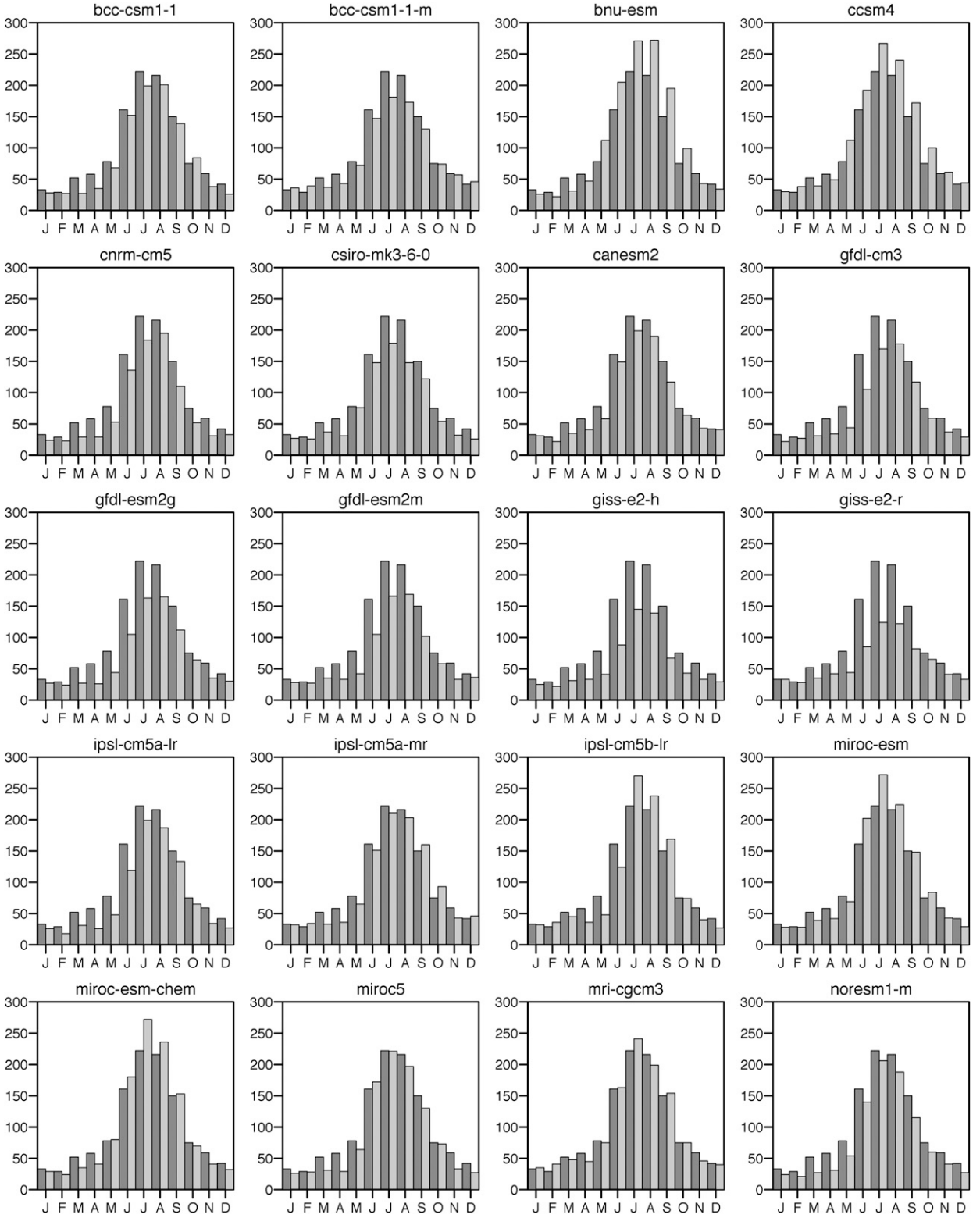


FIG. 7. Histograms illustrating the observed (dark gray) and predicted (light gray) monthly frequency of extreme-precipitation days during the 1970–99 period.

predicts a distinct peak in the frequency of extreme precipitation between June and September, with more than 50% of all extreme-precipitation days occurring during this 4-month period. The monthly and total frequencies of extreme-precipitation days vary substantially among the different models, however. For example, the CCSM4 model predicts 267 July extreme-precipitation days and 1344 total extreme-precipitation days during the 1970–99 period, whereas the GISS-E2-H model predicts only 124 July extreme-precipitation days and 734 total extreme-precipitation days. Although the predicted frequency of extreme precipitation does not appear to be strongly correlated with model resolution, it is worth noting that the models with intermediate resolutions yield the largest biases in extreme-precipitation frequency. As Fig. 8 suggests, the analog method as applied to the CMIP5 simulations generally underestimates the observed frequency of extreme precipitation in all months. This dry bias is most pronounced in late autumn/early winter (November–December) and early spring (March–April).

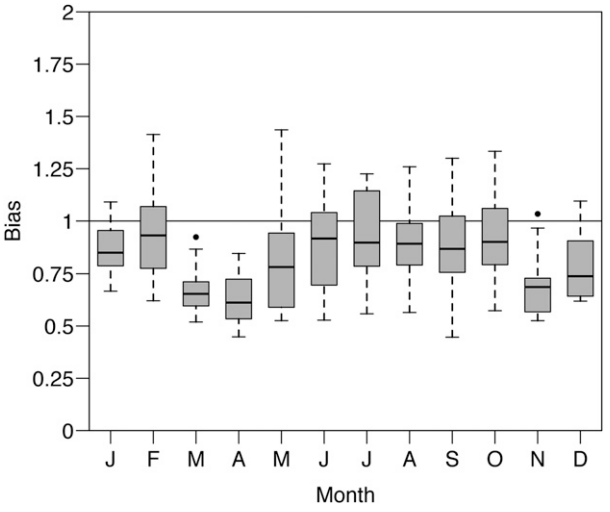


FIG. 8. Monthly bias in the frequency of extreme-precipitation days as predicted by the analog method during the 1970–99 period. Filled black circles outside the whiskers denote outliers.

### *b. Analysis of rarely selected analogs*

As the results above indicate, the analog method tends to underestimate historical precipitation extremes—in particular, for stations in groups 1, 2, and 4. The discrepancies between observed and downscaled precipitation extremes were investigated through a closer examination of the selection of candidate analogs. If certain historical synoptic weather patterns are not reproduced by the AOGCM simulations, it is likely that the exclusion of such candidate analogs may introduce a bias in predicted precipitation extremes, especially if some of the largest precipitation events occur on these analog days. Such analogs were found by isolating candidate analog days with extreme precipitation that were rarely selected by the CMIP5 models. To qualify as ''rarely selected,'' a given analog day cannot appear as a suitable analog (i.e., one of the 30 closest analogs on any given model day) in more than 4 (20%) of the 20 CMIP5 historical simulations. Overall, 82 unique analog days spanning the 1961–2010 period met the above criterion.

After the subset of rarely selected analog days was obtained, the distribution of PDS precipitation amounts reported on these analog days was compared with the distribution of all PDS precipitation amounts during the 1970–99 period. The comparison was carried out for each station group, as well as the entire study domain. As Fig. 9 illustrates, the PDS precipitation amounts from the subset of rarely selected analog days are generally larger than the PDS precipitation amounts from all extreme-precipitation days during the 1970–99 period. These differences are especially pronounced in groups 1, 2, and 4. For example, among the group-1 and group-2 stations, roughly 40% of PDS precipitation amounts on rarely selected analog days exceed 100 mm, whereas only 15%–20% of PDS precipitation amounts on all extreme-precipitation days during the 1970–99 period exceed 100 mm. Among the group-4 stations, nearly 50% of PDS precipitation amounts on rarely selected analog days exceed 75 mm, whereas only 15% of PDS precipitation amounts on all extreme-precipitation days during the 1970–99 period exceed 75 mm.

Of the 82 rarely selected analog days, nearly all (80) fell between June and October, with a distinct maximum (36) in September. This period coincides with the most active portion of the tropical-cyclone season in the Atlantic Ocean, suggesting that landfalling tropical cyclones (TCs) may be a common feature among the rarely selected analogs. A recent study by Kunkel et al. (2012) found that precipitation associated with TCs accounted for 35% of summer (June–August) 1-day 5-yr precipitation events and 44% of autumn (September–November) 1-day 5-yr precipitation events in the northeastern United States between 1908 and 2009. Moreover, given their relative proximity to the coast, stations in groups 1, 2, and 4 are generally more vulnerable to heavy precipitation associated with Atlantic TCs than stations in groups 3 and 5 are. To investigate the types of historical synoptic weather patterns associated with extreme precipitation that are not adequately replicated by the CMIP5 models, synoptic composite maps were created for the 82 rarely selected analog days. Before generating the composites, the 82 individual analog days were partitioned into clusters on the basis of similarities in the TPW, IVT, and $\zeta_{850}$ fields. To be more specific, standardized RMSE values were calculated

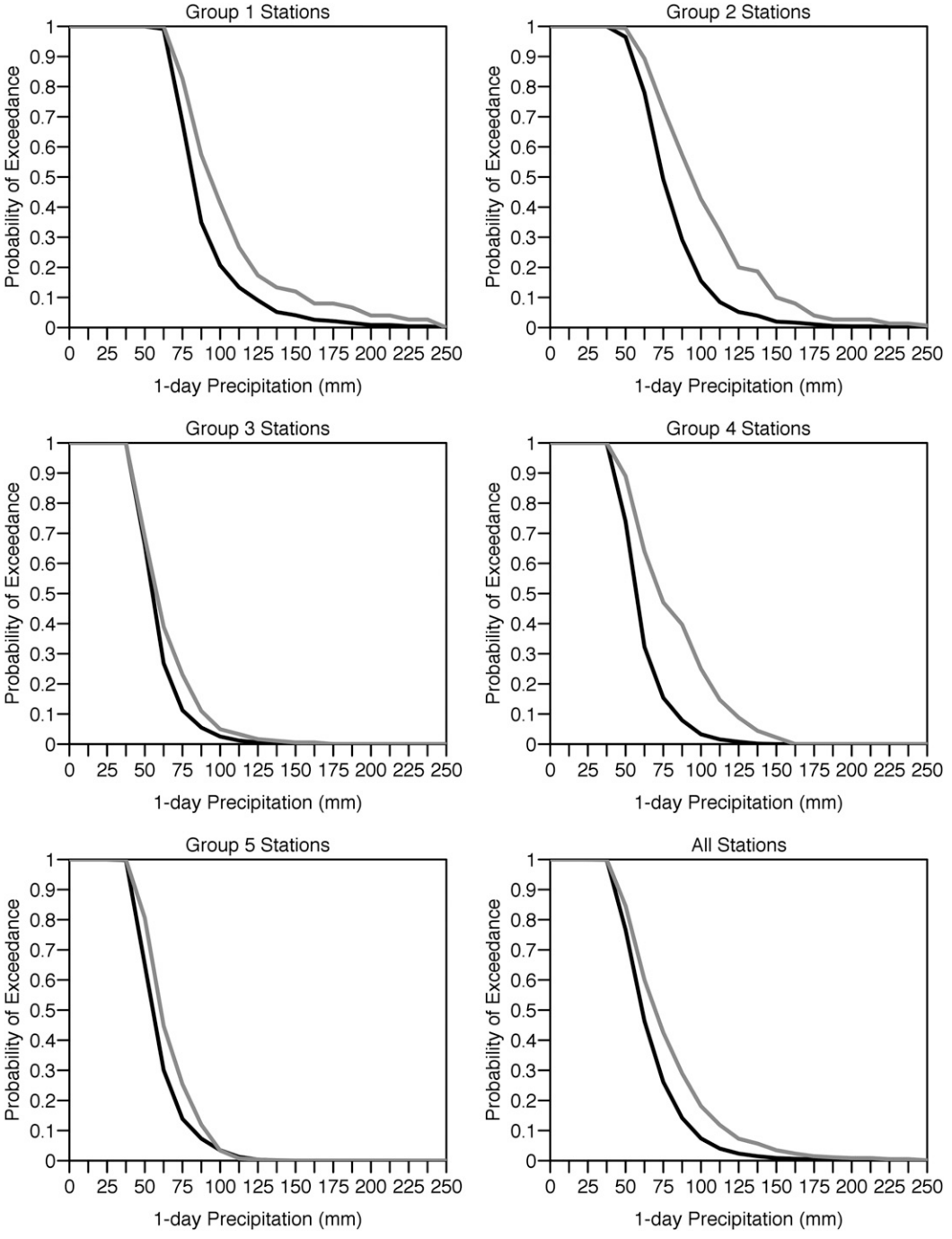


FIG. 9. Exceedance probabilities corresponding to all PDS precipitation amounts during the 1970–99 period (black lines) and the subset of PDS precipitation amounts on rarely selected analog days (gray lines).

for all unique pairs of analog days using the same method that was described in section 2b. Next, these standardized RMSE values were used to construct a distance matrix, and Ward's method of hierarchical clustering was subsequently applied to the resulting distance matrix. Eight distinct synoptic clusters were identified.

Supplemental storm-track, satellite, precipitation, and radar data were employed to elucidate the role of TCs and other meteorological causes of extreme precipitation [extratropical cyclones, fronts, mesoscale convective systems (MCSs), etc.] on these analog days. For the purpose of this study, the following four

categories were used to describe the meteorological cause of extreme precipitation on a given analog day: 1) precipitation directly or indirectly associated with a TC or posttropical cyclone (PTC), 2) precipitation associated with extratropical cyclones and/or frontal boundaries, 3) precipitation associated with MCSs, and 4) precipitation associated with airmass convection. The first category includes predecessor rain events (PREs; Cote 2007), as well as PTCs that have either undergone extratropical transition or become remnant lows within the previous 24 h. The last category refers to isolated or widely scattered convection occurring in an unstable air mass in the absence of a frontal boundary or surface cyclone. The existence of a TC within the analog search domain on a given day was verified using the International Best Track Archive for Climate Stewardship (IBTrACS) database (Knapp et al. 2010). Interpolated daily precipitation maps (provided by the Northeast Regional Climate Center), archived NEXRAD images (provided by the Iowa Environmental Mesonet), and archived geostationary satellite images (provided by the National Climatic Data Center, now known as the National Centers for Environmental Information) gave us valuable information about the intensity, type (i.e., convective vs stratiform), and spatial pattern of precipitation.

Figures 10 and 11 show synoptic composite maps for each of the eight clusters of rarely selected analog days. The cluster-1 composites (number of members $n = 11$) depict an 850-hPa ridge over the southeastern United States, with a large region of westerly moisture transport extending across the midwestern and northeastern United States (Fig. 10a). A weak surface cyclone is located over Lake Superior, just downstream of a positively tilted 850-hPa short-wave trough (Fig. 11a). Extreme precipitation on these analog days was primarily associated with airmass convection, an MCS, or organized convection in the warm sector of an extratropical cyclone. The cluster-2 composites ($n = 17$) show a similar pattern, but the 850-hPa ridge is located farther east and the short-wave trough near the Canada–U.S. border is neutral and more amplified (Fig. 10b). The resulting southwesterly low-level flow transports moist air from the lower Mississippi and Ohio Valleys into the Great Lakes states and helps to establish a thermal ridge over southeastern Canada via warm advection. Meanwhile, a potent warm-season extratropical cyclone is located over southern Canada (Fig. 11b). Extreme precipitation on these analog days was primarily associated with airmass convection and organized convection in the warm sector of an extratropical cyclone. One unique feature of the cluster-2 composites is a local maximum in TPW near the Florida Panhandle. Upon further inspection, 12 of the 17 analog days in cluster 2 featured a TC located over the northern Gulf of Mexico or the Gulf Coast states.

The cluster-3 composites ($n = 5$) are characterized by an intense 850-hPa cutoff low and associated surface cyclone centered over Lake Ontario (Figs. 10c and 11c). The surface cyclone is located near the poleward exit region of a 300-hPa jet streak. An extensive ring of cyclonically curved IVT surrounds the 850-hPa cutoff low, with pronounced meridional moisture transport along its eastern periphery. Extreme precipitation on these analog days was associated with strong extratropical cyclones and landfalling TCs undergoing extratropical transition [Agnes (1972)]. The cluster-4 composites ($n = 10$) depict a broad 850-hPa trough over the upper Midwest and a pronounced 850-hPa ridge and surface anticyclone over the Canadian Maritime Provinces (Figs. 10d and 11d). A region of enhanced meridional moisture transport parallels the Appalachian Mountains in advance of a tongue of moist air extending northward from the southeastern United States. This region of enhanced IVT terminates near the equatorward entrance region of a 300-hPa jet streak over southeastern Canada, placing the northeastern United States in a favorable location for quasi-geostrophic (QG) forcing for ascent. Extreme precipitation on these analog days was primarily associated with PREs, organized convection in the warm sector of an extratropical cyclone, and frontal passages.

The cluster-5 composites ($n = 9$) are characterized by an 850-hPa cutoff low near the South Carolina coast, a strong anticyclone over the northwestern Atlantic Ocean, and a region of vigorous poleward moisture transport between those two features (Fig. 10e). The 850-hPa cutoff low is collocated with a closed circulation in the sea level pressure (SLP) field and lies just west of a nearly symmetrical region of very moist air (TPW values approaching 60 mm; Fig. 11e). Upon further inspection, 6 of the 9 analog days in cluster 5 featured a landfalling TC along the Atlantic coast of the southeastern United States [David (1979), Gloria (1985), Hugo (1989), Floyd (1999), Hannah (2008), and Nicole (2010)]. Extreme precipitation on these analogs days was primarily associated with PREs or the TCs themselves. The cluster-6 composites ($n = 13$) show an 850-hPa short-wave trough and associated weak surface cyclone over the eastern United States (Figs. 10f and 11f). A region of enhanced IVT is coincident with a tongue of moist air extending northward along the East Coast. Extreme precipitation on these analog days was primarily associated with landfalling TCs that were undergoing extratropical transition and the remnants of landfalling TCs.

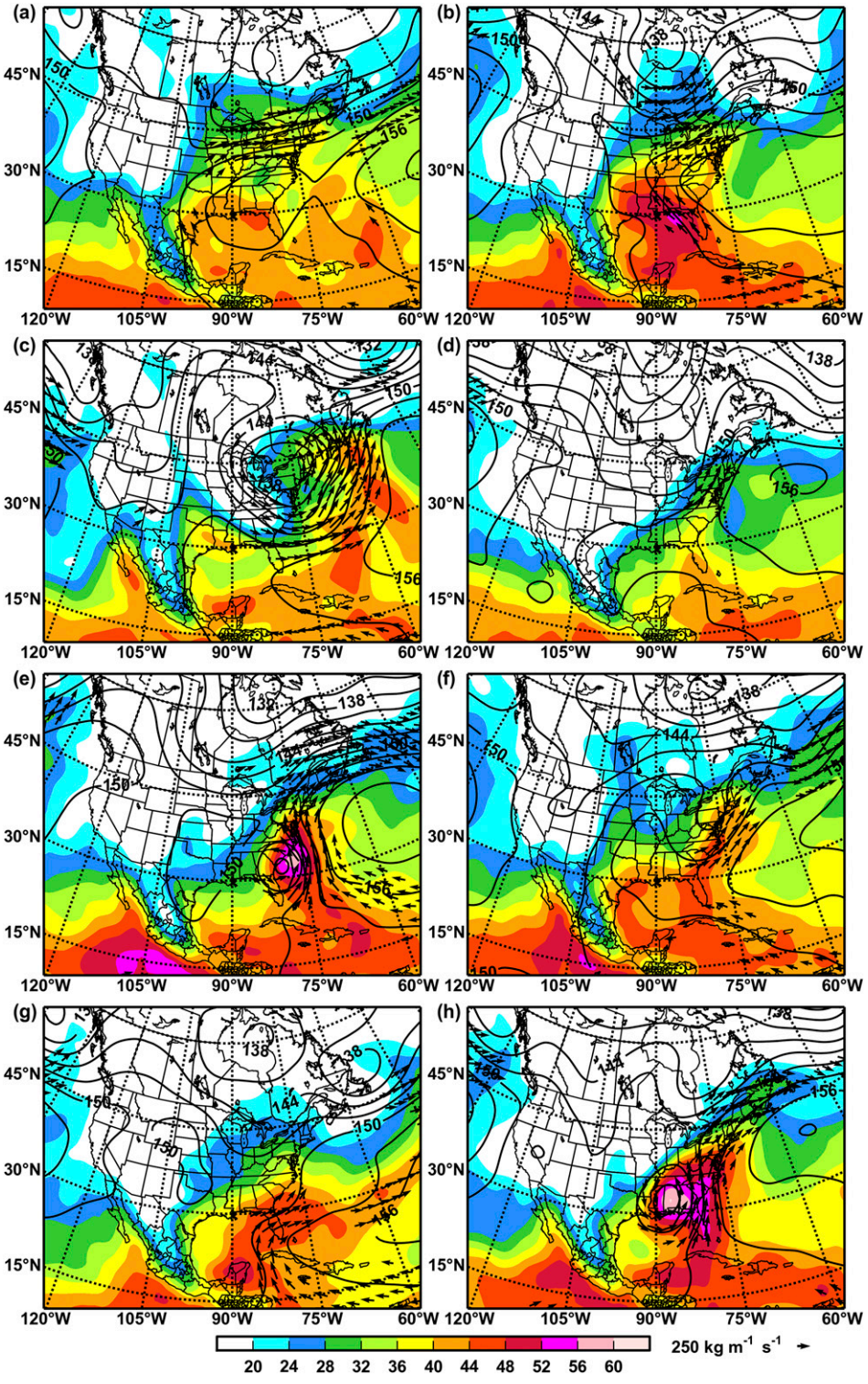


FIG. 10. Composite maps of TPW (shaded; every 4 mm), 850-hPa geopotential height (contours; every 6 dam), and IVT (arrows; values $\geq 250\,\mathrm{kg\,m^{-1}\,s^{-1}}$ only) for each of the eight clusters of rarely selected analog days.

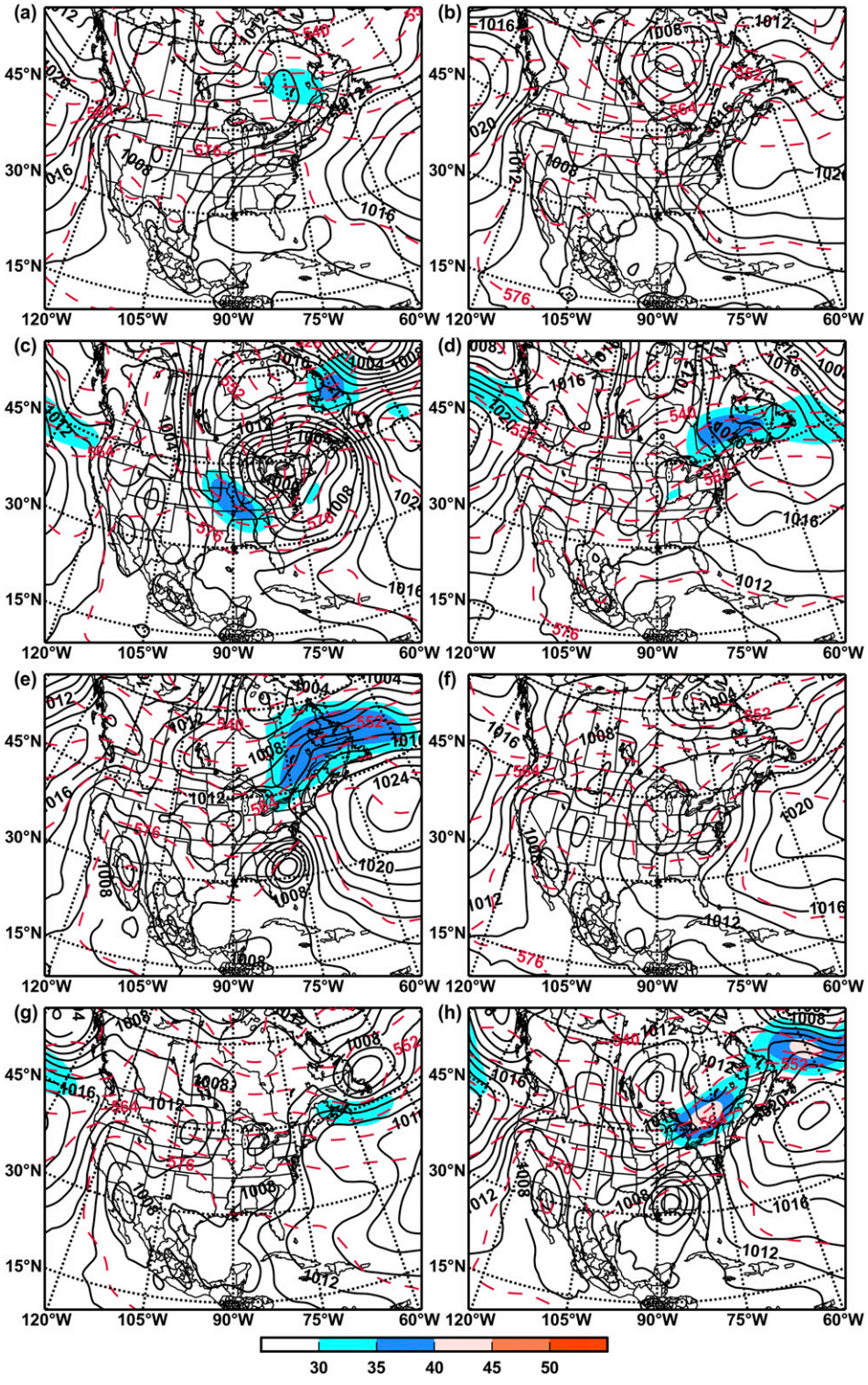


FIG. 11. Composite maps of 300-hPa scalar wind speed (shaded; every 5 m s$^{-1}$), mean SLP (solid contours; every 2 hPa), and 1000–500-hPa thickness (dashed contours; every 6 dam) for each of the eight clusters of rarely selected analog days.

The cluster-7 composites ($n = 9$) depict an 850-hPa short-wave trough and a weak area of surface low pressure over the Great Lakes states (Figs. 10g and 11g). A region of strong meridional moisture transport extends from the western Caribbean Sea northward to Florida, but the magnitude of IVT over the northeastern United States is notably weaker than in the previous composites. Extreme precipitation on these analog days was primarily associated with PREs and extratropical cyclones over the Great Lakes region. The cluster-8 composites ($n = 8$) are characterized by an 850-hPa cutoff low over the eastern Gulf Coast states and a large swath of pronounced moisture transport extending from Florida to the Canadian Maritimes (Fig. 10h). The 850-hPa cutoff low is collocated with a region of extremely moist air (TPW values approaching 60 mm) and a closed circulation in the SLP field, which suggests that a TC has recently made landfall near the Florida Panhandle. North of the TC, a 300-hPa jet streak over southeastern Canada places the eastern Great Lakes states in a favorable region for QG forcing for ascent (Fig. 11h). Upon further inspection, 6 of the 8 analog days in cluster 8 featured a landfalling TC in the southeastern United States [Opal (1995), Isidore (2002), Frances (2004), Ivan (2004), and Katrina (2005)]. Extreme precipitation on these analog days was either directly or indirectly (i.e., a PRE scenario) related to the landfalling TC.

Overall, 55 (67%) of the 82 rarely selected analog days featured a TC within the analog search domain. This number includes TCs located over the northwestern Atlantic Ocean or the Gulf of Mexico, as well as landfalling TCs in the central and eastern United States. An additional 6 analog days featured PTCs that either underwent extratropical transition or dissipated into remnant lows during the previous 24 h. As Fig. 12 illustrates, certain models are more likely to reproduce synoptic patterns associated with rarely selected analog days than others. For instance, more than 25% of rarely selected analog days appear as suitable analogs when the analog search algorithm is run for the BCC_CSM1.1, CCSM4, IPSL-CM5B-LR, and MRI-CGCM3 models. Meanwhile, fewer than 5% of rarely selected analog days appear as suitable analogs when the analog search algorithm is run for the BNU-ESM, GFDL-ESM2G, GFDL-ESM2M, IPSL-CM5A-LR, IPSL-CM5A-MR, and NorESM1-M models. The likelihood of reproducing rarely selected analog patterns does not appear to be strongly correlated with model resolution. When the rarely selected analog days are partitioned into days with and without a TC in the analog search domain, it becomes clear that certain models are less likely to reproduce analog patterns associated with TC days than those associated with non-TC days (e.g., CCSM4), and vice versa (e.g., IPSL-CM5B-LR).

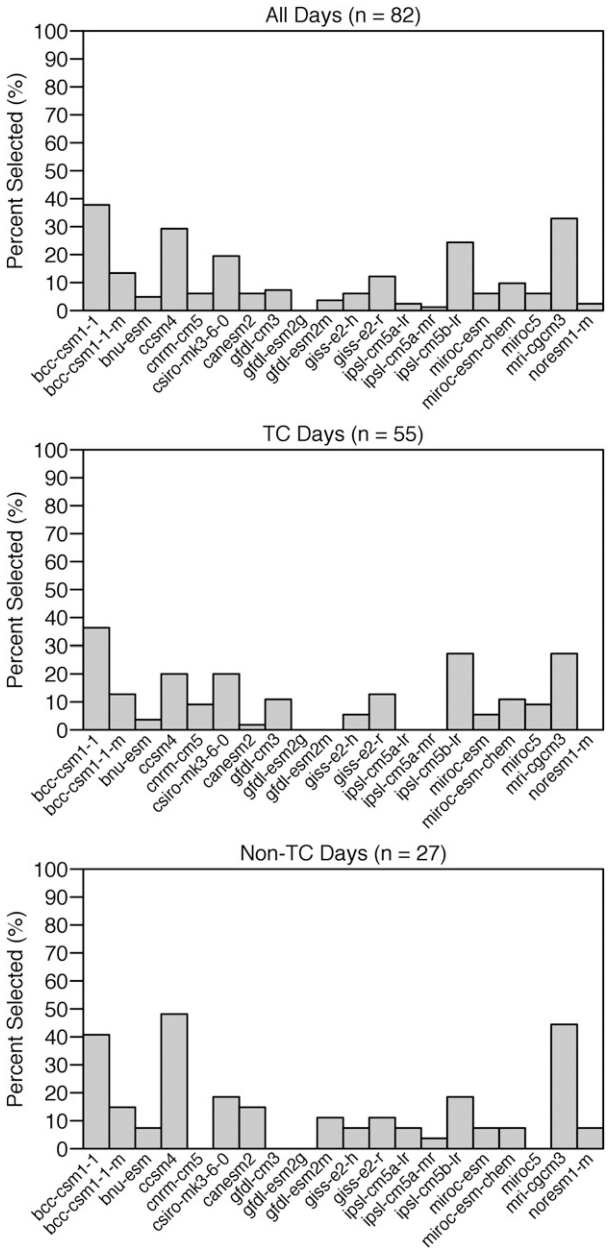


FIG. 12. Bar plots showing the percentage of rarely selected analog days that appear as suitable analogs for each CMIP5 model.

Not surprising is that TCs and PTCs were the leading meteorological cause of extreme precipitation on rarely selected analog days. Extreme precipitation occurring on 39% of rarely selected analog days could be directly or indirectly (i.e., a PRE scenario) attributed to a TC or PTC. Extratropical cyclones and frontal boundaries were associated with extreme precipitation on 34% of rarely selected analog days. In these cases, extreme precipitation

resulted primarily from organized convection in the warm sector of the surface cyclone or along an associated cold front. Airmass convection and MCSs were responsible for extreme precipitation on 12% and 7% of rarely selected analog days, respectively. Extreme precipitation on the remaining analog days was associated with remnant moisture from previously existing TCs.

## 4. Conclusions

This study evaluates a multistep approach for downscaling daily precipitation extremes from AOGCM simulations using historical analogs. Unlike most analog downscaling techniques, this method estimates daily precipitation amounts only on model days for which the closest historical analogs predict the occurrence of extreme precipitation. Overall, the analog method yields realistic estimates of historical precipitation extremes and compares favorably to the dynamically downscaled CORDEX and NARCCAP simulations.

One advantage of this downscaling approach is that it can be used to assess the ability of AOGCMs to replicate synoptic weather patterns that are commonly associated with extreme precipitation. For instance, the composite analysis of rarely selected analogs revealed that TCs were a prominent feature on rarely selected analog days. This result is consistent with previous studies, which have demonstrated that coarse-scale AOGCMs struggle to adequately simulate TC activity in the North Atlantic basin (Camargo 2013; Walsh et al. 2013). Given these shortcomings, it may be worthwhile to investigate whether applying the analog method to high-resolution climate models can reduce biases in simulated weather patterns and downscaled precipitation extremes. Recent studies by Knutson et al. (2013) and Mei et al. (2014) suggest that increasing model resolution alone can indeed yield promising results with respect to simulating Atlantic TC activity. Another advantage of the analog method is that it can offer insights as to how the frequency distribution of synoptic weather patterns associated with extreme precipitation may change in the future. By extension, changes in simulated large-scale circulation patterns and/or moisture variables could provide a physical basis for explaining projected changes in extreme precipitation.

Any conclusions drawn from applications to historical and future climate-model simulations must acknowledge several important caveats. First, although the analog method may produce realistic estimates of historical precipitation extremes, there is no guarantee that the synoptic weather patterns associated with extreme precipitation are replicated well by the models. Second, the meteorological causes of extreme precipitation vary by region, and the predictor variables must therefore be chosen accordingly. Analog predictors that are well suited to the northeastern United States may not be appropriate in other regions such as the southwestern United States or Central America. Third, this particular downscaling procedure only estimates precipitation on days for which the selected historical analog day is an extreme-precipitation day. Therefore, unlike other statistical downscaling methods, it is not possible to evaluate certain metrics of daily precipitation variability, such as wet-day fraction, spatial autocorrelation, and temporal autocorrelation [see Gutmann et al. (2014) and He et al. (2016) for examples of how these metrics are typically evaluated]. Fourth, as is the case with any statistical downscaling approach, the analog method relies on the assumption of stationarity. This assumption may be rendered invalid if the meteorological forcing and/or atmospheric conditions associated with extreme precipitation change over time. Last, because the analog method uses historical precipitation observations, future precipitation extremes will ultimately be constrained by the existing climate record. Increases in return-period values can only result from a resampling of observed precipitation amounts, potentially leading to an underestimation of changes in the upper tail of the extreme-precipitation distribution (Boé et al. 2006).

*Acknowledgments.* This work was supported by the New York State Energy Research and Development Authority (Contract 28257), with partial support from NOAA Contract EA133E07CN0090 and the New York State Agricultural Experiment Station.

## REFERENCES

Allen, R. J., and A. T. DeGaetano, 2005: Areal reduction factors for two eastern United States regions with high rain-gauge density. *J. Hydrol. Eng.*, **10**, 327–335, doi:10.1061/(ASCE)1084-0699(2005)10:4(327).

Archambault, H. M., L. F. Bosart, D. Keyser, and A. R. Aiyyer, 2008: Influence of large-scale flow regimes on cool-season precipitation in the northeastern United States. *Mon. Wea. Rev.*, **136**, 2945–2963, doi:10.1175/2007MWR2308.1.

Benestad, R. E., 2010: Downscaling precipitation extremes: Correction of analog models through PDF predictions. *Theor. Appl. Climatol.*, **100**, 1–21, doi:10.1007/s00704-009-0158-1.

Boé, J., L. Terray, F. Habets, and E. Martin, 2006: A simple statistical-dynamical downscaling scheme based on weather types and conditional resampling. *J. Geophys. Res.*, **111**, D23106, doi:10.1029/2005JD006889.

Brekke, L., B. L. Thrasher, E. P. Maurer, and T. Pruitt, 2013: Downscaled CMIP3 and CMIP5 climate and hydrology projections: Release of downscaled CMIP5 projections, comparison with preceding information, and summary of user needs. U.S. Dept. of the Interior Bureau of Reclamation Rep., 47 pp. [Available online at http://gdo-dcp.ucllnl.org/downscaled_cmip_projections/techmemo/downscaled_climate.pdf.]

Camargo, S. J., 2013: Global and regional aspects of tropical cyclone activity in the CMIP5 models. *J. Climate*, **26**, 9880–9902, doi:10.1175/JCLI-D-12-00549.1.

Castellano, C. M., and A. T. DeGaetano, 2016: A multi-step approach for downscaling daily precipitation extremes from historical analogues. *Int. J. Climatol.*, **36**, 1797–1807, doi:10.1002/joc.4460.

Christensen, J. H., and O. B. Christensen, 2003: Climate modelling: Severe summertime flooding in Europe. *Nature*, **421**, 805–806, doi:10.1038/421805a.

Cote, M. R., 2007: Predecessor rain events in advance of tropical cyclones. M.S. thesis, Dept. of Atmospheric and Environmental Sciences, University at Albany, State University of New York, 200 pp.

Dayan, U., K. Nissen, and U. Ulbrich, 2015: Review article: Atmospheric conditions inducing extreme precipitation over the eastern and western Mediterranean. *Nat. Hazards Earth Syst. Sci.*, **15**, 2525–2544, doi:10.5194/nhess-15-2525-2015.

DeGaetano, A. T., 1998: A Smirnov test-based clustering algorithm with application to extreme precipitation data. *Water Resour. Res.*, **34**, 169–176, doi:10.1029/97WR03133.

——, 2009: Time-dependent changes in extreme-precipitation return-period amounts in the continental United States. *J. Appl. Meteor. Climatol.*, **48**, 2086–2099, doi:10.1175/2009JAMC2179.1.

Eden, J. M., and M. Widmann, 2014: Downscaling of GCM-simulated precipitation using model output statistics. *J. Climate*, **27**, 312–324, doi:10.1175/JCLI-D-13-00063.1.

Gao, X., C. A. Schlosser, P. Xie, E. Monier, and D. Entekhabi, 2014: An analogue approach to identify heavy precipitation events: Evaluation and application to CMIP5 climate models in the United States. *J. Climate*, **27**, 5941–5963, doi:10.1175/JCLI-D-13-00598.1.

Groisman, P. Ya., R. W. Knight, and T. R. Karl, 2012: Changes in intense precipitation over the central United States. *J. Hydrometeor.*, **13**, 47–66, doi:10.1175/JHM-D-11-039.1.

Gutiérrez, J. M., D. San-Martín, S. Brands, R. Manzanas, and S. Herrera, 2013: Reassessing statistical downscaling techniques for their robust application under climate change conditions. *J. Climate*, **26**, 171–188, doi:10.1175/JCLI-D-11-00687.1.

Gutmann, E., T. Pruitt, M. P. Clark, L. Brekke, J. R. Arnold, D. A. Raff, and R. M. Rasmussen, 2014: An intercomparison of statistical downscaling methods used for water resources assessments in the United States. *Water Resour. Res.*, **50**, 7167–7186, doi:10.1002/2014WR015559.

Haylock, M. R., G. C. Cawley, C. Harpham, R. L. Wilby, and C. M. Goodess, 2006: Downscaling heavy precipitation over the United Kingdom: A comparison of dynamical and statistical methods and their future scenarios. *Int. J. Climatol.*, **26**, 1397–1415, doi:10.1002/joc.1318.

He, X., N. W. Chaney, M. Schleiss, and J. Sheffield, 2016: Spatial downscaling of precipitation using adaptable random forests. *Water Resour. Res.*, **52**, 8217–8237, doi:10.1002/2016WR019034.

Heideman, K. F., and J. M. Fritsch, 1988: Forcing mechanisms and other characteristics of significant summertime precipitation. *Wea. Forecasting*, **3**, 115–130, doi:10.1175/1520-0434(1988)003<0115:FMAOCO>2.0.CO;2.

Heineman, M., 2012: Trends in precipitation maxima at U.S. Historical Climatology Network stations: 1893–2010. *Proc. World Environmental and Water Resources Congress 2012*, Albuquerque, NM, American Society of Civil Engineers, 2003–2012, doi:10.1061/9780784412312.201.

Hidalgo, H. G., M. D. Dettinger, and D. R. Cayan, 2008: Downscaling with constructed analogues: Daily precipitation and temperature fields over the United States. California Energy Commission Public Interest Energy Research Program Rep. CEC-500-2007-123, 62 pp. [Available online at http://www.energy.ca.gov/2007publications/CEC-500-2007-123/CEC-500-2007-123.PDF.]

Hosking, J. R. M., and J. R. Wallis, 1997: *Regional Frequency Analysis: An Approach Based on L-Moments.* Cambridge University Press, 244 pp.

Imbert, A., and R. E. Benestad, 2005: An improvement of analog model strategy for more reliable local climate change scenarios. *Theor. Appl. Climatol.*, **82**, 245–255, doi:10.1007/s00704-005-0133-4.

IPCC, 2014: Summary for policymakers. *Climate Change 2014: Impacts, Adaptation, and Vulnerability*, C. B. Field et al., Eds., Cambridge University Press, 1–32. [Available online at http://www.ipcc.ch/pdf/assessment-report/ar5/wg2/ar5_wgII_spm_en.pdf.]

Jones, C., F. Giorgi, and G. Asrar, 2011: The Coordinated Regional Downscaling Experiment: CORDEX—An international downscaling link to CMIP5. *CLIVAR Exchanges*, No. 56, International CLIVAR Project Office, Southampton, United Kingdom, 34–40. [Available online at http://www.clivar.org/sites/default/files/documents/Exchanges56.pdf.]

Junker, N. W., R. H. Grumm, R. Hart, L. F. Bosart, K. M. Bell, and F. J. Pereira, 2008: Use of normalized anomaly fields to anticipate extreme rainfall in the mountains of northern California. *Wea. Forecasting*, **23**, 336–356, doi:10.1175/2007WAF2007013.1.

Kalnay, E., and Coauthors, 1996: The NCEP/NCAR 40-Year Reanalysis Project. *Bull. Amer. Meteor. Soc.*, **77**, 437–471, doi:10.1175/1520-0477(1996)077<0437:TNYRP>2.0.CO;2.

Karl, T. R., J. M. Melillo, and T. C. Peterson, Eds., 2009: *Global Climate Change Impacts in the United States*. Cambridge University Press, 189 pp.

Knapp, K. R., M. C. Kruk, D. H. Levinson, H. J. Diamond, and C. J. Neumann, 2010: The International Best Track Archive for Climate Stewardship (IBTrACS): Unifying tropical cyclone data. *Bull. Amer. Meteor. Soc.*, **91**, 363–376, doi:10.1175/2009BAMS2755.1.

Knutson, T. R., and Coauthors, 2013: Dynamical downscaling projections of twenty-first-century Atlantic hurricane activity: CMIP3 and CMIP5 model-based scenarios. *J. Climate*, **26**, 6591–6617, doi:10.1175/JCLI-D-12-00539.1.

Konrad, C. E., 1997: Synoptic-scale features associated with warm season heavy rainfall over the interior southeastern United States. *Wea. Forecasting*, **12**, 557–571, doi:10.1175/1520-0434(1997)012<0557:SSFAWW>2.0.CO;2.

Kunkel, K. E., 2003: North American trends in extreme precipitation. *Nat. Hazards*, **29**, 291–305, doi:10.1023/A:1023694115864.

——, K. Andsager, and D. R. Easterling, 1999: Long-term trends in extreme precipitation events over the conterminous United States and Canada. *J. Climate*, **12**, 2515–2527, doi:10.1175/1520-0442(1999)012<2515:LTTIEP>2.0.CO;2.

——, D. R. Easterling, D. A. R. Kristovich, B. Gleason, L. Stoecker, and R. Smith, 2012: Meteorological causes of the secular variations in observed extreme precipitation events for the conterminous United States. *J. Hydrometeor.*, **13**, 1131–1141, doi:10.1175/JHM-D-11-0108.1.

——, L. E. Stevens, S. E. Stevens, L. Sun, E. Janssen, D. Wuebbles, and J. G. Dobson, 2013: Regional trends and scenarios for the U.S. national climate assessment: Part 9. Climate of the contiguous United States. NOAA Tech. Rep. NESDIS 142-9, 85 pp.

[Available online at https://www.nesdis.noaa.gov/sites/default/files/asset/document/NOAA_NESDIS_Tech_Report_142-9-Climate_of_the_Contiguous_United_States.pdf.]

LaPenta, K. D., and Coauthors, 1995: The challenge of forecasting heavy rain and flooding throughout the Eastern Region of the National Weather Service. Part I: Characteristics and events. *Wea. Forecasting*, **10**, 78–90, doi:10.1175/1520-0434(1995)010<0078:TCOFHR>2.0.CO;2.

Lorenz, E. N., 1969: Atmospheric predictability as revealed by naturally occurring analogues. *J. Atmos. Sci.*, **26**, 636–646, doi:10.1175/1520-0469(1969)26<636:APARBN>2.0.CO;2.

Maddox, R. A., C. F. Chappell, and L. R. Hoxit, 1979: Synoptic and meso-α scale aspects of flash flood events. *Bull. Amer. Meteor. Soc.*, **60**, 115–123, doi:10.1175/1520-0477-60.2.115.

Maraun, D., and Coauthors, 2010: Precipitation downscaling under climate change: Recent developments to bridge the gap between dynamical models and the end user. *Rev. Geophys.*, **48**, RG3003, doi:10.1029/2009RG000314.

Matulla, C., X. Zhang, X. L. Wang, J. Wang, E. Zorita, S. Wagner, and H. von Storch, 2008: Influence of similarity measures on the performance of the analog method for downscaling daily precipitation. *Climate Dyn.*, **30**, 133–144, doi:10.1007/s00382-007-0277-2.

Mearns, L. O., W. J. Gutowski, R. Jones, L.-Y. Leung, S. McGinnis, A. M. B. Nunes, and Y. Qian, 2009: A regional climate change assessment program for North America. *Eos, Trans. Amer. Geophys. Union*, **90**, 311–312, doi:10.1029/2009EO360002.

Meehl, G. A., C. Covey, T. Delworth, M. Latif, B. McAvaney, J. F. B. Mitchell, R. J. Stouffer, and K. E. Taylor, 2007: The WCRP CMIP3 multimodel dataset: A new era in climate change research. *Bull. Amer. Meteor. Soc.*, **88**, 1383–1394, doi:10.1175/BAMS-88-9-1383.

Mei, W., S. Xie, and M. Zhao, 2014: Variability of tropical cyclone track intensity in the North Atlantic: Observations and high-resolution simulations. *J. Climate*, **27**, 4797–4814, doi:10.1175/JCLI-D-13-00587.1.

Murphy, J., 1999: An evaluation of statistical and dynamical techniques for downscaling local climate. *J. Climate*, **12**, 2256–2284, doi:10.1175/1520-0442(1999)012<2256:AEOSAD>2.0.CO;2.

Perica, S., and Coauthors, 2013: Precipitation-frequency atlas of the United States. NOAA Atlas 14, Vol. 9, version 2.0, 43 pp. [Available online at http://www.nws.noaa.gov/oh/hdsc/PF_documents/Atlas14_Volume9.pdf.]

Ribalaygua, J., L. Torres, J. Pórtoles, R. Monjo, E. Gaitán, and M. R. Pino, 2013: Description and validation of a two-step analogue/regression downscaling method. *Theor. Appl. Climatol.*, **114**, 253–269, doi:10.1007/s00704-013-0836-x.

Smith, J. A., G. Villarini, and M. L. Baeck, 2011: Mixture distributions and the hydroclimatology of extreme rainfall and flooding in the eastern United States. *J. Hydrometeor.*, **12**, 294–309, doi:10.1175/2010JHM1242.1.

Taylor, K. E., R. J. Stouffer, and G. A. Meehl, 2012: An overview of CMIP5 and the experiment design. *Bull. Amer. Meteor. Soc.*, **93**, 485–498, doi:10.1175/BAMS-D-11-00094.1.

Tryhorn, L., and A. T. DeGaetano, 2011: A comparison of techniques for downscaling extreme precipitation over the northeastern United States. *Int. J. Climatol.*, **31**, 1975–1989, doi:10.1002/joc.2208.

van den Dool, H. M., 1994: Searching for analogues, how long must we wait? *Tellus*, **46A**, 314–324, doi:10.3402/tellusa.v46i3.15481.

——, J. Huang, and Y. Fan, 2003: Performance and analysis of the constructed analogue method applied to U.S. soil moisture over 1981–2001. *J. Geophys. Res.*, **108**, 8617, doi:10.1029/2002JD003114.

Villarini, G., J. A. Smith, and G. A. Vecchi, 2013: Changing frequency of heavy rainfall over the central United States. *J. Climate*, **26**, 351–357, doi:10.1175/JCLI-D-12-00043.1.

Walsh, K., S. Lavender, E. Scoccimarro, and H. Murakami, 2013: Resolution dependence of tropical cyclone formation in CMIP3 and finer resolution models. *Climate Dyn.*, **40**, 585–599, doi:10.1007/s00382-012-1298-z.

Ward, J. H., 1963: Hierarchical grouping to optimize an objective function. *J. Amer. Stat. Assoc.*, **58**, 236–244, doi:10.1080/01621459.1963.10500845.

Wetterhall, F., S. Halldin, and C.-Y. Xu, 2005: Statistical precipitation downscaling in central Sweden with the analogue method. *J. Hydrol.*, **306**, 174–190, doi:10.1016/j.jhydrol.2004.09.008.

Wilby, R. L., and T. M. L. Wigley, 1997: Downscaling general circulation model output: A review of methods and limitations. *Prog. Phys. Geogr.*, **21**, 530–548, doi:10.1177/030913339702100403.

——, C. W. Dawson, and E. M. Barrow, 2002: SDSM—A decision support tool for the assessment of regional climate change impacts. *Environ. Modell. Software*, **17**, 145–157, doi:10.1016/S1364-8152(01)00060-3.

——, S. P. Charles, E. Zorita, B. Timbal, P. Whetton, and L. O. Mearns, 2004: Guidelines for use of climate scenarios developed from statistical downscaling methods. IPCC Task Group on Data and Scenario Support for Impact and Climate Analysis Rep., 27 pp. [Available online at http://www.ipcc-data.org/guidelines/dgm_no1_v1_10-2003.pdf.]

Wilks, D. S., 1993: Comparison of three-parameter probability distributions for representing annual extreme and partial duration precipitation series. *Water Resour. Res.*, **29**, 3543–3549, doi:10.1029/93WR01710.

——, and R. P. Cember, 1993: Atlas of precipitation extremes for the northeastern United States and southeastern Canada. Northeast Regional Climate Center Research Rep. RR 93-5, 40 pp. [Available online at http://www.nrcc.cornell.edu/services/research/reports/RR_93-5.pdf.]

Winkler, J. A., 1988: Characteristics of summertime extreme rainstorms in Minnesota. *Ann. Assoc. Amer. Geogr.*, **78**, 57–73, doi:10.1111/j.1467-8306.1988.tb00191.x.

Zorita, E., and H. von Storch, 1999: The analog method as a simple statistical downscaling technique: Comparison with more complicated methods. *J. Climate*, **12**, 2474–2489, doi:10.1175/1520-0442(1999)012<2474:TAMAAS>2.0.CO;2.